

# Ignition scaling laws and their application to capsule design

*M. C. Herrmann, M. Tabak, and J. D. Lindl*

This article was submitted to  
42<sup>nd</sup> Annual Meeting of the Division of Plasma Physics  
Quebec City, Canada  
October 23-27, 2000

**October 20, 2000**

*U.S. Department of Energy*

Lawrence  
Livermore  
National  
Laboratory

# Ignition scaling laws and their application to capsule design

Mark C. Herrmann, Max Tabak, John D. Lindl

*Box 808 L-018*

*Lawrence Livermore National Laboratory*

*Livermore, California 94550*

*(July 4, 2003)*

## Abstract

This paper investigates the amount of energy required to ensure the ignition of an inertial confinement fusion (ICF) capsule. In the first part, a series of one dimensional LASNEX [G. B. Zimmerman and W. L. Kruer, *Plasma Phys. Controlled Fusion* **2**, 51 (1975)] simulations is performed to create a database of barely ignited capsules that span the parameter regime of interest. This database is used to develop scaling laws for the ignition energy in terms of both the stagnated capsule parameters and the inflight capsule parameters, and to explore the connection between these two parameter sets. The second part of this paper examines how much extra energy is required to overcome the effect of the inevitable surface imperfections that are amplified during the implosion process. These perturbations can lead to break up of the capsule in flight or to mix of cold fuel into the hotspot, both of which can cause the capsule to fail. As an example, a family of capsules with fixed adiabat, drive pressure, and absorbed energy is studied; the capsule from this family that is maximally robust to these failure modes is found.

## 1. INTRODUCTION

How much energy is needed to robustly ignite a given inertial confinement fusion capsule? This is of considerable interest in the optimization of an inertial fusion driver, since the energy the driver must supply is a monotone function of the energy required in the capsule. The yield of the capsule will typically exhibit a behavior like that shown in Fig. 1 (dark curve), as the imploding fuel energy is increased the capsule yield increases slowly until the ignition energy is reached, after which the yield rapidly increases to some value and remains there. For the purposes of this paper, the ignition energy ( $E_{ign}$ ) is defined as the fuel energy where the capsule gain (capsule yield over capsule absorbed energy) equals one. In the first part of this paper the dependency of  $E_{ign}$  on the various parameters of the capsule implosion will be examined by creating a database of barely ignited capsules, and fitting a scaling law to this data. Much of this work summarizes previous work by the authors<sup>1</sup> investigating

the energy required for ignition, which in turn was prompted by discrepancies in computational scaling laws found by Levedahl and Lindl<sup>2</sup> and Basko and Johner.<sup>3</sup>

In the absence of perturbations, a capsule would be designed with an energy just above  $E_{ign}$  so that the maximum capsule gain would be achieved. However, in the presence of perturbations, the yield curve typically shifts to higher energy as seen in Fig. 1 (light curve). Thus, in order to get the full yield, the capsule must be designed with some margin relative to the unperturbed ignition energy. However, for fixed driving pressure and energy budget, there is a conflict between increasing the implosion velocity (and margin) and the increased hydrodynamic instability growth associated with it. In the second part of this paper we will examine the tradeoffs between increased margin and increased instability in a family of capsules with fixed absorbed energy, drive temperature, and adiabat.

## II. IGNITION SCALING LAW

### A. Capsule Parameters

Before investigating the energy required for ignition it is useful to understand what independent variables matter for capsule implosions (and therefore can matter for the ignition energy).

After the shocks have passed through the capsule, and the peak drive power is reached, a typical capsule implosion approaches a state of uniformly accelerating equilibrium (see Fig. 2). This state can be described by solving the hydrodynamic equations in the limit of a thin shell:

$$\rho g = -\nabla p, p(r_0) = P, \rho(r) = \alpha \rho^{5/3} \quad \text{---}$$

$$\rho(r) = \rho_{peak} \left( 1 + \frac{2(r-r_0)}{5\Delta} \right)^{3/2}, r > r_0 - \frac{5}{2}\Delta \quad \text{---}$$

$$v(r) = \text{const}, \Delta \equiv \frac{m}{4\pi\rho_{peak}r_0^2} \quad \text{---}$$

where  $P$  is the applied pressure,  $\rho_{peak} = (P/\alpha)^{3/5}$  and the fuel is assumed to be isentropic (in practice, capsules are not perfectly isentropic, although capsules which are well pulse shaped are nearly so). The capsule will remain in this state until spherical effects (such as convergence or the back pressure of the fill gas) begin to matter. If only capsules that have a fixed initial gas fill, almost all of their ablator ablated (at time of peak implosion velocity), and nearly isentropic fuel are considered, the

implosion can be characterized by four parameters:  $m$ , the fuel mass;  $P$ , the drive pressure;  $\alpha_{if}$ , the inflight value of the adiabat (the ratio of the fuel pressure to the Fermi degenerate pressure); and  $v$ , the peak implosion velocity. These four quantities uniquely define a uniformly accelerating equilibrium. The yield of an inertial confinement fusion (ICF) capsule can be thought of as a function of these four parameters. Note that capsules that have capsule gain equal to one will occupy a three dimensional (3D) hyperplane in this 4D space.

Following Lindl, Chapter 5,<sup>4</sup> these four parameters can be related to the capsule stability. By energy conservation

$$PV \sim mv^2 \quad (4)$$

Take  $r_0$  to be the radius where the peak drive begins, and  $\Delta r_0$  to be the capsule shell thickness at this radius, then this can be written:

$$\frac{4\pi r_0^3}{3} P \sim 4\pi r_0^2 \Delta r_0 \rho v^2 \quad (5)$$

The ratio of the radius where peak drive begins to the shell thickness at that radius is:

$$\frac{r_0}{\Delta r_0} \equiv IFAR \sim v^2 \frac{\rho}{P} \sim \frac{v^2}{c_s^2} \equiv M^2 \quad (6)$$

$$IFAR \sim v^2 \alpha_{if}^{-3/5} P^{-2/5} \quad (7)$$

where  $M$  is the Mach number, and the adiabatic relation has been used to write  $c_s$  in terms of  $\alpha_{if}$  and  $P$ . The in flight aspect ratio (IFAR) is a well known measure of capsule stability, the higher the IFAR the more unstable the capsule. Note that in deriving this relation mass ablation has been neglected (which is appropriate for direct drive, but inappropriate for indirect drive), however, even when significant mass ablation is present IFAR can be written in terms of  $v$ ,  $\alpha_{if}$ , and  $P$  (Lindl, Chapter 5).<sup>4</sup>

## B. The Isobaric Model

After the imploding capsule converges sufficiently far the shell begins to stagnate on the gas at the center. The detailed profiles at this time become more complicated because: electron conduction, bremsstrahlung and fusion burn all become important in addition to the complicated hydrodynamics of a spherically converging compressible shell. As the capsule stagnates it converts its kinetic energy

into pressure, and goes from an implosion that is supersonic to a stagnated state that is subsonic. As was understood by Meyer-ter-Vehn,<sup>5</sup> this means that the capsule will become isobaric. Stagnated capsules typically have two distinct regions, a high-temperature, lower-density (still hundreds of times solid density) hot spot and a higher-density, low-temperature cold fuel region. A simple model for the ignition energy can be developed by: assuming the fuel is isobaric, requiring the hot spot have a minimum temperature, and requiring the hot spot have a minimum  $\rho r$ .<sup>5</sup> Since the velocity of the imploding shell can be related to the hydrodynamic stability of the implosion,<sup>4</sup> the minimum energy for “ignition” is expressed in terms of the implosion velocity. This leads to the well known scaling law for the ignition energy<sup>6</sup>:

$$E_{ign} \propto \frac{\alpha_{stag}^3}{v^{10}} \quad (8)$$

where  $\alpha_{stag}$  is the adiabat of the stagnated cold fuel, which may differ from the in flight adiabat ( $\alpha_{if}$ ).

### C. Methodology

We must find a large number of marginally ignited capsules with values of  $m$ ,  $v$ ,  $\alpha_{if}$ , and  $P$  that span the range of interest for inertial confinement fusion. Tuning enough radiation driven capsules to get a meaningful database of marginally ignited capsules would be prohibitively time consuming. We choose to consider capsules that are composed of deuterium tritium (DT) fuel only and are driven with a time varying pressure source applied on their outer surface. While care must still be taken to achieve a pulse that maintains the fuel as isentropic as possible, it turns out that this is much easier than tuning a radiation driven capsule.

The initial state of such a capsule is shown in Fig. 3. Four parameters are used to specify a calculation: the mass of the fuel,  $m$ ; the initial fuel aspect ratio,  $\zeta = R_{in}/(R_{out} - R_{in})$ ; the strength of the initial shock,  $p_0$ ; and the maximum drive pressure,  $P$ . These four quantities can be related to the four parameters mentioned previously, with  $m$  and  $P$  being obvious,  $p_0$  determines the capsule adiabat  $\alpha_{if}$  and  $\zeta$  and  $m$  can be used to determine the capsule volume which from Eq. 4 determines the implosion velocity. The DT gas fill is kept at  $3 \times 10^{-4} \text{g/cm}^3$  for the capsules considered in this study. This is equivalent to a fixed initial cryogenic fuel temperature about  $1.5^\circ \text{K}$  below the DT triple point.

To successfully implode these capsules, a pulse shape that goes from  $p_0$  to  $P$  for a given  $m$  and  $\zeta$  is needed. This pulse shape must be designed to keep the fuel as isentropic as possible. If the inner fuel layers are not isentropic, the stagnation of the shell will be affected and the amount of energy required to ignite the capsule will increase. The pulse shape chosen also must mimic, as much as possible, the pressure versus time at the fuel-ablator interface in radiation driven capsules.

A generic pulse shape chosen to accomplish these goals is shown in Fig. 4. The four shocks and ramp mimic the pressure at the ablator DT interface for typical radiation driven capsules. The four shocks are timed with an adaptive pulse shaper. The pulse shaper monitors the transit of the shocks through the capsule and launches subsequent shocks so that they do not overtake the previous shock and that long rarefactions between shocks are avoided. The fuel remains quite isentropic. A typical entropy profile achieved by this pulse shaper is shown in Fig. 5.

In accord with previous studies,<sup>2,3</sup> a capsule is considered ignited if the fusion yield is eight times the work done on the capsule. (The factor of 8 accounts for the typical hydrodynamic efficiency of a radiation driven implosion, which is about 12%.) To find the barely ignited capsules a one dimensional (1D) binary search over  $\zeta$  (starting with initial values which give a subignited and superignited capsule) is performed. This typically takes between 10 and 20 LASNEX<sup>7</sup> runs. Once a barely ignited capsule is found, the run is postprocessed to measure several variables of interest, which are then stored in a database of marginally ignited capsules (see Reference 1 for more details).

To ensure that these pressure-driven DT-only implosions mimic radiation driven capsules, radiation driven capsules and pressure driven capsules with similar values of  $m$ ,  $v$ ,  $\alpha_{if}$  and  $P$  have been compared. As can be seen from Fig. 6, which shows the density and pressure profiles of the two capsules at stagnation time, the stagnated states are quite similar.

Using the above prescription, about one hundred marginally ignited capsules were found over a range of parameter space of interest for ICF (masses from 0.04 to 5 mg,  $p_0$  from 0.5 to 8 Mbar, and  $P$  from 30 to 250 Mbar, which corresponds to marginally ignited capsules with  $v$  from 2.0 to  $5.0 \times 10^7$  cm/sec,  $\alpha_{if}$  from 0.6 to 3.0, and  $E_{ign}$ , from 3.5 to 350 kJ).

#### D. Scaling Law Using $\alpha_{stag}$

Using the theoretical scaling law Eq. 8 as a model the database was fit to a power law of the form:

$$E_{fit}(\alpha_{stag}, v) = C \frac{\alpha_{stag}^a}{v^b} \quad (9)$$

Since the relative error is of more interest than the absolute error, the logarithm of Eq. 9 is taken and a linear least squares method is used to find the  $(a, b, C)$  which minimizes:

$$\sum_i \left( \log E_{fit}^i - a \log \alpha_{stag}^i + b \log v^i - \log C \right)^2 \quad (10)$$

A best fit scaling law for the ignition energy was found to be:

$$E_{fit} \text{ (kJ)} = 2.1 \alpha_{stag}^{2.66 \pm 0.06} \left( \frac{v}{3 \times 10^7 \text{ cm/sec}} \right)^{-7.21 \pm 0.11} \quad (11)$$

A histogram showing the distribution of  $E_{ign}/E_{fit}$  for the capsules in this study is shown in Fig. 7. This fit compares favorably with the errors seen in similar studies.<sup>2,3</sup>

### E. Increase in the Adiabatic Index During Stagnation

While the scaling law listed in Eq. 11 is useful, the adiabat at stagnation is not something which is directly under a capsule designer's control, unlike the four parameters listed in Section IIA. Of course, if the capsule stagnation were adiabatic ( $\alpha_{stag} \sim \alpha_{if}$ ),  $\alpha_{if}$  could be substituted for  $\alpha_{stag}$  in Eq. 11. To assess the degree to which stagnation is adiabatic the evolution of  $\alpha$  was studied. Fig. 8 shows a series of snapshots showing the evolution of the adiabat versus fuel mass, from the time of peak implosion velocity (lowest curve) to the time of stagnation (highest curve). Three important features are 1) a gradual increase in the value of  $\alpha$  before stagnation (which is due to DT's deviations from an ideal  $\gamma = 5/3$  gas), 2) the gradual increase in adiabat which occurs for both the shocked and unshocked fuel after stagnation begins, and 3) the rapid change in adiabat versus fuel mass which is due to the stagnation shock propagating out through the fuel.

The first of these can be understood by examining the QEOS<sup>8</sup> equation of state for DT which was used in these calculations. Note that the pressure at the time of peak implosion velocity ranges from 30 to 250 Mbar. In this pressure range, DT has a  $\gamma$  slightly higher than 5/3. The pressure at stagnation time is in the 100's of Gbar. At these very large pressures, DT approaches an ideal  $\gamma = 5/3$  gas. Thus even under isentropic compression,  $\alpha \propto p/\rho^{5/3}$  will increase from the time of peak implosion velocity to stagnation time.

The second effect mentioned above is due mainly to the deposition of energy from fusion neutrons created by the burning hot spot. While these neutrons are not coupling much energy to the fuel due to their long ranges, they do dominate over all sources other than the stagnation shock. Both

$\alpha$ -particle deposition and electron conduction occur over too short a range to significantly affect fuel far from the hot spot. At typical hot spot temperatures near stagnation time (8 keV) the bremsstrahlung power is 6 times lower than the neutron power. Furthermore the energetic photons created by the bremsstrahlung (with energies on the order of the electron temperature) typically have ranges in deuterium-tritium plasmas longer than a 14 MeV neutron range.

The effect of the stagnation shock on the capsule adiabat can be studied in self-similar solutions for hollow spherical shells.<sup>9,10</sup> These analytical solutions behave in many ways like a stagnating ICF capsule. For shells coming in at high Mach number (as in ICF), the stagnation shock is launched when the shell hits the axis, this shock then propagates out from the center leaving an isobaric region of material which is essentially stopped behind it. The density and pressure versus radius at different times from such an implosion are shown in Fig. 9. The Mach number for this implosion is 8.5. The stagnation shock starts at the axis at  $t = 0$  and propagates back through the fuel. Meyer-ter-Vehn *et al.*<sup>9,10</sup> found that for a  $\gamma = 5/3$  gas, the pressure and density of a fluid element after the stagnation shock passed can be related to the pressure and density of the same fluid element at  $t = 0$ :

$$P_f \sim P_0 M^3 \quad (12)$$

$$\rho_f \sim \rho_0 M^{3/2} \quad (13)$$

where  $M$  is the Mach number of the implosion. This implies:

$$\alpha_{stag} \sim \frac{P_f}{\rho_f^{5/3}} \sim \frac{P_0}{\rho_0^{5/3}} \sqrt{M} \quad (14)$$

$$\Rightarrow \alpha_{stag} \sim \alpha_{if} \sqrt{M} \sim \alpha_{if}^{0.85} v^{0.5} P^{-0.1} \quad (15)$$

where the sound speed is written in terms of the pressure,  $P$ , and the inflight adiabat,  $\alpha_{if}$ ,

( $c_s \propto \sqrt{P/\rho}$ ,  $\rho \propto P^{3/5} / \alpha_{if}^{3/5}$ ) when substituting for the Mach number. This suggests the adiabat increase during stagnation depends on the  $\alpha_{if}$ ,  $v$ , and  $P$ .

In order to understand the combined effect of the three processes the database of marginally ignited capsules was fit to find the increase of the adiabat during stagnation. Following the example of Eq. 15 we fit  $\alpha_{stag}$  using  $\alpha_{if}$ ,  $v$ , and  $P$ :

$$\alpha_{stag} = 3.2 \alpha_{if}^{0.75 \pm 0.01} \left( \frac{v}{3 \times 10^7 \text{ cm/sec}} \right)^{0.44 \pm 0.03} \times \left( \frac{P}{100 \text{ Mbar}} \right)^{-0.21 \pm 0.01} \quad (16)$$

which is not too different from the scaling law in Eq. 15.

To get a scaling law for the ignition energy in terms of parameters which the capsule designer can control Eq. 16 is substituted into Eq. 11 yielding

$$E_{fit} \sim \alpha_{if}^{2.00} v^{-6.04} P^{-0.56} \quad (17)$$

More generally the barely ignited database can be fit to a scaling law which includes the  $\alpha_{if}$ ,  $v$ , and  $P$ .

This gives

$$E_{fit} \alpha_{if} (\text{kJ}) = 50.8 \alpha_{if}^{1.88 \pm 0.05} \left( \frac{v}{3 \times 10^7 \text{ cm/sec}} \right)^{-5.89 \pm 0.12} \times \left( \frac{P}{100 \text{ Mbar}} \right)^{-0.77 \pm 0.03} \quad (18)$$

which has a standard deviation similar to that of Eq. 11 (see Fig. 10). This scaling law is quite similar to Eq. 17, except for a slightly stronger inverse pressure dependence. Actually, if the drive pressure had been included as parameter in the fit with  $\alpha_{stag}$  (Eq 11), there would have been a  $P^{-0.22}$  dependence to the scaling law. Together with Eq. 17 this accounts for all of the pressure dependence in Eq. 18. While most of the effect of the pressure on the ignition energy comes by way of its effect on the increase in the adiabat during stagnation, some must arise from a change in the fuel configuration at stagnation time.

## F. Comparisons to Radiation Driven Capsules and Previous Scaling Laws

In order to ensure that the scaling law is valid it has been compared to radiation driven capsules and previous computational scaling laws. In Fig. 11 we compare the imploding fuel energy of several marginally ignited radiation driven and directly driven capsules to the ignition energy predicted by the scaling law of Eq. 18 using the capsules' values of  $v$ ,  $\alpha_{if}$ , and  $P$ . Over a large range of masses the scaling law does quite a good job of predicting the ignition energy. Note that the spread in the data is consistent with the spread in the data for the pressure driven capsules.

The generalized scaling law in Eq. 18 also explains discrepancies seen in previous computational studies<sup>2,3</sup> which were not understood. Levedahl and Lindl<sup>2</sup> and Basko and Johner<sup>3</sup> found that if the drive pressure is kept constant, as the implosion velocity and fuel adiabat of the capsule under consideration are varied, the minimum ignition energy scales like  $E_{\text{ign}} \sim \alpha_{\text{if}}^{1.7}/\nu^{5.5}$ . In contrast, Basko and Johner found that when the pressure is varied in a hydrodynamically similar way which preserves the implosion Mach number ( $P \sim \alpha_{\text{if}}^{-3/2} \nu^5$ ), the ignition energy scales like  $E_{\text{ign}} \sim \alpha_{\text{if}}^{3.0}/\nu^{9.1}$ .

Note that the dependence of  $E_{\text{fit } \alpha_{\text{if}}}$  in Eq. 18 on the pressure explains much of the difference between these two results:

$$E_{\text{fit } \alpha_{\text{if}}} \sim \alpha^{1.9} \nu^{-5.9} \text{ for } P \text{ constant} \quad (19)$$

$$E_{\text{fit } \alpha_{\text{if}}} \sim \alpha^{3.0} \nu^{-9.6} \text{ for } P \sim \alpha^{-3/2} \nu^5 \quad (20)$$

### G. Implications

The scaling law can be used to examine the tradeoff between energy, power, and stability. Solving Eq. 7 for  $\nu$  and substituting the result into Eq. 18 gives:

$$E_{\text{ign}} \sim \frac{\alpha_{\text{if}}^{1.8}}{\nu^6 P^{0.8}} \sim \frac{1}{IFAR^3 P^2} \quad (21)$$

Thus to lower the energy required for ignition IFAR or  $P$  must increase. In general, however, IFAR has some upper limit set by stability considerations and  $P$  has an upper limit set by the driver power intensity (or for the case of laser drivers, laser plasma interactions), and thus the minimum energy for ignition is set. Surprisingly the adiabat drops out implying, at least in the simplest case where only the IFAR determines the stability, there is no advantage to operating at high adiabat in order to achieve ignition. Of course these comments are true only in the limit where Eq. 7 is valid.

### III. CAPSULE OPTIMIZATION

How can this scaling law for the ignition energy be used to aid in the design of capsules? For a given driver energy we may want to design a capsule with the maximum gain or we may want a

capsule that is maximally robust to perturbations. In this section we will investigate, with the aid of the scaling law, how capsule perturbations affect the design of these two capsules.

In order to simplify this problem somewhat, consider the case where the adiabat and drive pressure are fixed. (It seems likely, given Eq. 7 and Eq. 18 that both the capsule gain and robustness will be maximized by operating at the highest pressure possible. Furthermore in the absence of perturbations the capsule gain and the capsule margin are maximized at the lowest possible adiabat. In the presence of perturbations, operating at the lowest adiabat may not maximize gain and performance<sup>11</sup> but we do not consider that case here.) Furthermore, we assume the coupling efficiency of driver energy to fuel energy is nearly fixed so that the capsule fuel energy is also fixed.

A space of fuel energy versus velocity is shown in Fig. 12. Contours of constant mass are shown in dashed lines. Since the adiabat and drive pressure are fixed, the ignition energy from Eq. 18 is just a function of velocity, and in the absence of perturbations the space can be divided into a region of no ignition (below the dark line) and ignition (above the dark line). The light line shows a line of constant fuel energy. Thus the optimization question posed above becomes where on this line is the gain or the robustness maximized in the presence of perturbations. In general to maximize the gain, we want to implode the largest mass that ignites, thus the capsule would operate very near where the ignition curve intersects the energy curve. In contrast, for maximum robustness, we would want the maximum distance between the capsule and the ignition cliff, thus the capsule would operate at the maximum velocity possible.

The presence of perturbations changes this thinking. For the case of maximum gain, capsule imperfections grow during the implosion and can cause mix of cold fuel into the hot spot. This can delay ignition which, if the capsule is close to the ignition cliff, can cause the capsule to fail. Thus capsules are typically designed with 1D margin relative to the ignition energy so that additional energy is available to ameliorate the effects of mix. However, the higher implosion velocity requires larger IFAR, as seen from Eq. 7. As IFAR increases the capsule may suffer from shell break up during the implosion and fail to ignite. There is a maximum gain and an optimum robustness between these two limits.

For a concrete example consider an indirectly driven plastic ablator capsule which is of interest for heavy ion driven inertial confinement fusion because capsules with plastic ablator may be significantly easier to mass produce than the beryllium ablator capsules used in many previous designs.<sup>12,13</sup> The capsule considered is shown in Fig. 13. It has a nominal outer radius of 2.3 mm, absorbs approximately 900 kJ of energy and is driven with a pulse shape that has a foot temperature

of 80 eV and a peak drive of around 265 eV. The gas fill is taken to be  $6 \times 10^{-4} \text{ g/cm}^3$ , which is close to the vapor pressure at the DT triple point.

To study the optimization consider four variants of this capsule, labeled Slow, Moderate, Fast, and Very Fast. The capsules are designed so that they have the same foot and peak drive temperature (although the pulse shapes differ) and they absorb the same amount of energy to within 1%. The main difference is the amount of DT fuel mass each different variant has, as can be seen in Fig. 14. The position in energy-velocity space for the four capsules is shown in Fig. 15. The capsules do not lay precisely on the constant energy line due to variations in the hydrodynamic efficiencies of the implosions. Several parameters for these capsules are shown in Table 1.

The 1D margin is defined as the amount of fuel energy in the implosion divided by how much energy is required to barely ignite that capsule mass (graphically this is where the dashed lines in Fig. 15 intersect the ignition cliff). These parameters follow the trends expected from above. The Slow capsule has high yield, low IFAR, and low margin, and the Very Fast capsule has nearly half the yield and twice the IFAR of the Slow capsule. However, it has significantly more 1D margin.

The consequences of little 1D margin can be seen in the behavior of the unperturbed capsules in Fig. 16. The central ion temperature is plotted parametrically versus the  $(\rho r)$  of the hot spot for the four capsules. The capsules start cold and move towards higher temperatures, while assembling their hot spot. Note that the short dashed curve (Slow capsule) reaches some maximum value of  $(\rho r)$  and then its  $(\rho r)$  starts to decrease before the capsule ignites. Thus the capsule is igniting as it expands after peak compression. During ignition,  $\alpha$ -deposition heats the fuel while electron conduction and radiation losses cool it. If a capsule ignites while it is imploding, the hydrodynamic work helps heat the fuel. If it ignites during expansion the  $\alpha$ -deposition must overcome the hydrodynamic losses in addition to electron conduction and radiation losses. In such circumstances a slight delay due to the mix of cold fuel into the hot spot (which lowers the temperature and therefore the reaction rate) can quench ignition. In contrast the Very Fast capsule (solid curve) is still assembling its hot spot when it reaches ignition temperatures.

The consequences of high IFAR can be seen in Fig. 17, which shows results from two dimensional (2D) single mode growth factor calculations for the four capsules versus Legendre mode number. These curves were created by seeding very small perturbations of the appropriate wavelength on the outside of the plastic at  $t = 0$ . The implosion was then done and at the time of peak implosion velocity the size of the perturbation at the plastic-DT interface was measured and compared to the initial perturbation size in order to get a growth factor. As we move from Slow to

Very Fast the peak of the spectrum moves from mode number 50 to mode number 90. At the same time, the growth factor increases by a factor of six. This growth factor is a measure of how susceptible the various capsules are to shell break up.

Another important indicator for capsules is the amount of growth that occurs at the hot spot-cold fuel interface near ignition time. This is significantly different from the growth at peak implosion velocity on the outside of the capsule, since the perturbations must feed through the shell and because these modes grow during the deceleration of the capsule. The net effect is to shift the growth to lower mode numbers. In Fig. 18 the single mode growth factors at the hot spot interface at ignition time are plotted. While the Very Fast capsule does have the highest overall growth peaking above 2000 in mode 40, it is interesting to see that the slow capsule has higher growth rates than the moderate capsule for almost all the mode numbers and even has higher growth factors than the Fast and Very Fast capsules for mode 15. This occurs because the slow capsule undergoes extra deceleration (and therefore extra deceleration growth) before it ignites due to the ignition delay discussed earlier.

Which of these capsules is optimally robust? The answer will depend on the spectrum of perturbations initially present on the capsules. Thus we turn to multimode simulations in which a spectrum of modes is seeded with realistic amplitudes, on the outside of the ablator and on the inside of the DT ice layer and then do 2D simulations on a  $15^\circ$  wedge of the perturbed capsule, resolving modes 12 to 160. These calculations were carried out in a way analogous to those done for NIF capsules<sup>14,15</sup> taking advantage of a novel tabular weighted opacity scheme developed by Marinak *et al.*<sup>16</sup>

It is currently not known what the spectrum or amplitude of surface or ice perturbations will be on capsules of this scale, indeed it is not entirely clear how to scale results from measurements of current capsule surface roughness to the capsule scale of interest. For simplicity we choose to study capsules with the same ablator roughness spectrum and ice roughness spectrum which has been used in the design of NIF ignition scale capsules.<sup>14,15</sup> This spectrum has a nominal roughness of about 8 nm for the ablator surface (modes 1 to 160) and 1  $\mu\text{m}$  for the ice surface. To study the effect of increasing roughness we merely multiply the entire roughness spectrum by some number, thereby increasing the rms deviation of the surface from perfectly smooth. In Fig. 19 a color coded density plot for the four capsules near the time of peak implosion velocity is shown. These simulations assumed 80 nm ablator roughness and 1  $\mu\text{m}$  ice roughness. We find that the ice roughness does not feed out significantly, and thus is not a big contributor to the perturbations that are seen. Note that

the Very Fast capsule is perturbed significantly. The spike tips are at lower density than the rest of the fuel suggesting their entropy has been raised by radiation burning through the ablator. The bubbles are penetrating most of the way through the shell, suggesting that a rougher initial finish would have led to shell breakup. In contrast, the Slow capsule looks barely perturbed.

In Fig. 20, density plots for the same capsules and same roughnesses are shown near ignition time. In contrast to the time of peak velocity all of the perturbations seem to be of comparable size in the four capsules at this time. There is a trend towards higher mode number as we move from the Slow capsule to the Very Fast capsule. Of course the single mode growth factors at ignition time (seen in Fig. 18) show less variation between capsules than those at time of peak velocity which partly explains why the perturbation size scale is more similar. Another important effect is the nonlinear saturation of the instability, which becomes more important at small radii and at higher mode number.<sup>17</sup> Despite the perturbations seen here, all these capsules ignite and give a significant fraction of their clean yield.

A comparison of the capsule performance versus ablator roughness (see Fig. 21) provides the clearest indicator of the relative performance of each capsule. By examining the detailed simulations, we can conclude the Slow capsule fails due to perturbations sticking into the hot spot delaying the ignition. In contrast, for the Very Fast capsule the shell breaks up from the outside and swirls material in again causing ignition to fail. Both the Moderate and Fast capsules, which have margin 1.3 - 1.6 have significant yield up to 200 nm initial ablator roughness, making them about twice as robust as the Slow capsule and 1.6 times as robust as the Very Fast capsule. For reference, mandrels have been fabricated that have surface roughnesses for modes 11 and up in the range 10-20 nm.<sup>18</sup> This range is highlighted in Fig. 21. Although the Slow capsule can tolerate a lower maximum ablator roughness than the Moderate and Fast capsules, for surface roughnesses below 80 nm it gives the maximum gain. As the initial surface roughness increases, the capsule which gives maximum gain and the capsule which is the most robust become one and the same until eventually ignition becomes impossible for capsules with the absorbed energy under consideration.

#### **IV. DISCUSSION AND SUMMARY**

In summary, we have developed a generalized scaling law (Eq. 18) for the ignition energy of ICF capsules which accounts for the effect of the drive pressure. We have found the plastic capsule which

gives the maximum gain and the capsule that is maximally robust for a particular absorbed energy, adiabat, and drive pressure. The answer depends on the achievable surface finish. Future work will be to generalize the optimization to different absorbed energies, adiabats and drive pressures.

We have also done 2D stability calculations on high yield plastic ablator capsules which are of interest for inertial fusion energy and other high yield ICF applications. They appear to be significantly more robust than ignition scale targets, as they are able to withstand surface roughnesses from 10-20 times achieved mandrel finishes. This robustness might be used to relax the requirements for target fabrication. As an alternative capsules with higher IFAR (that require lower drive temperatures) might be designed. This would relax the driver power requirements.

### **ACKNOWLEDGMENTS**

The authors would like acknowledge useful discussions with T. Dittrich, S. Haan, and M. Marinak. This work was performed under the auspices of the United States Department of Energy by the University of California Lawrence Livermore National Laboratory under contract No. W-7405-Eng-48.

## REFERENCES

- <sup>1</sup>M.C. Herrmann, M. Tabak, and J.D. Lindl, Nucl. Fusion **41**, 99 (2001).
- <sup>2</sup>W.K. Levedahl and J.D. Lindl, Nucl. Fusion **37**, 165 (1997).
- <sup>3</sup>M.M. Basko and J. Johner, Nucl. Fusion **38**, 1779 (1998).
- <sup>4</sup>J.D. Lindl, *Inertial Confinement Fusion: The Quest for Ignition and Energy Gain Using Indirect Drive* (Springer-Verlag, New York, 1998).
- <sup>5</sup>J. Meyer-ter-Vehn, Nucl. Fusion **22**, 561 (1982).
- <sup>6</sup>M.D. Rosen, J.D. Lindl, and A.R. Thiessen, *Laser Programs Annual Report - 1983* (Lawrence Livermore National Laboratory, Livermore, CA, 1984), Chap. 3, pp. 5-9.
- <sup>7</sup>G.B. Zimmerman and W.L. Kruer, Plasma Phys. Controlled Fusion **2**, 51 (1975).
- <sup>8</sup>R.M. More, K.H. Warren, D.A. Young, and G.B. Zimmerman, Phys. Fluids **31**, 3059 (1988).
- <sup>9</sup>J. Meyer-ter-Vehn and C. Schalk, Z. Naturforsch. **37a**, 955 (1982).
- <sup>10</sup>J. Meyer-ter-Vehn, in *Proceedings of the 29th Scottish Universities Summer School in Physics: Laser-Plasma Interactions: 3*, edited by M. B. Hooper (Scottish Universities Summer School in Physics Publications and Institute of Physics Publishing, London, 1985), Vol. 14, pp. 234-245.
- <sup>11</sup>M. Tabak, D.H. Munro, and J.D. Lindl, Phys. Fluids B **25**, 1007 (1990).
- <sup>12</sup>M. Tabak and D. A. Callahan-Miller, Phys. Plasmas **5**, 1895 (1998).
- <sup>13</sup>D. A. Callahan-Miller and M. Tabak, Nucl. Fusion **39**, 1547 (1999).

<sup>14</sup>T.R. Dittrich, S.W. Haan, M.M. Marinak, *et al.*, Phys. Plasmas **5**, 3708 (1998).

<sup>15</sup>T.R. Dittrich, S.W. Haan, M.M. Marinak, *et al.*, Phys. Plasmas **6**, 2164 (1999).

<sup>16</sup>see National Technical Information Service Document DE-96004569 [M.M. Marinak, R.E. Tipton, B.A. Remington, S.W. Haan, S.V. Weber, in ICF Quarterly Report(1995), UCRL-LR-105821-95-3]. Copies may be ordered from National Technical Information Service, Springfield, VA 22161. (unpublished)

<sup>17</sup>S. Haan, Phys. Rev. A **39**, 5812 (1989).

<sup>18</sup>D. Goodin, Private Communication, 2000.

<sup>19</sup>D.E. Hinkel, S.W. Haan, and T.R. Dittrich, Bull. Am. Phys. Soc. **44**, 167 (1999).

<sup>20</sup>S.V. Weber, S.G. Glendinning, D.H. Kalantar, M.H. Key, B.A. Remington, E. Wolfrum, C.P. Verdon, and J.P. Knauer, Phys. Plasmas **4**, 1978 (1997).

<sup>21</sup>D.D.M. Ho, J.A. Harte, and M. Tabak, Nucl. Fusion **35**, 1125 (1995).

## FIGURE CAPTIONS

FIG. 1. Yield (a.u.) versus energy in imploding fuel for typical capsule.

FIG. 2. Density, pressure, and velocity profiles for a uniformly accelerating equilibrium.

FIG. 3. Generic structure of capsules used in this study.

FIG. 4. Generic form of pressure pulse shape used to drive fuel only capsules.

FIG. 5. Adiat profile vs. fuel mass at peak implosion velocity. Note  $\alpha$  can be less than unity during the transition from a solid to a high temperature plasma.

FIG. 6. A comparison of the stagnated states (at time of peak  $\rho_{\perp}$ ) of two marginally ignited capsules, one pressure driven and one radiation driven, with similar masses, entropy profiles, peak pressures, and implosion velocities.

FIG. 7. Distribution of the energy required for marginal ignition divided by the energy predicted by Equation 11 for the pressure driven capsules used in this study.

FIG. 8. Adiat of the fuel at different times, from time of peak implosion velocity to time of stagnation.

FIG. 9. Results from self-similar hollow shell spherical implosions with Mach number equal to 8.5,  $\gamma = 5/3$ .

FIG. 10. Distribution of the energy required for marginal ignition divided by the energy predicted by Equation 18 for the pressure driven capsules used in this study.

FIG. 11. Ratio of fuel energy for marginally ignited radiation and directly driven capsules to fit prediction from Eq. 18 using the capsules  $v$ ,  $\alpha_{if}$ , and  $P$  plotted versus fuel mass. The highlighted

points are a 350 eV drive temperature beryllium ablator capsule,<sup>19</sup> a direct drive (DD) high adiabat capsule,<sup>20</sup> and a high yield inertial fusion energy capsule.<sup>21,12</sup>

FIG. 12. Space of fuel energy versus implosion velocity. Contours of constant mass are dashed. The dark line shows the ignition energy for a fixed adiabat and drive pressure, the light line shows a line of constant energy.

FIG. 13. The radial build of the capsule being optimized.

FIG. 14. The four capsules under consideration from left to right: Very Fast, Fast, Moderate, Slow.

FIG. 15. The four capsule under consideration, in fuel energy, velocity space. From left to right: Slow, Moderate, Fast, Very Fast.

FIG. 16. Central  $T_i$  vs.  $\rho_-$  of the hot spot for four capsules. Very Fast (solid), Fast (long dashes), Moderate (long and short dashes), and Slow (short dashes).

FIG. 17. Single mode growth factors measured at the plastic DT interface at time of peak velocity for the four capsules. Very Fast (dashed gray), Fast (solid black), Moderate (solid gray), and Slow (dashed black).

FIG. 18. Single mode growth factors measured at the hot spot interface at time of ignition for the four capsules. Very Fast (dashed gray), Fast (solid black), Moderate (solid gray), and Slow (dashed black).

FIG. 19. Color-coded plot of density versus position from multimode simulations near time of peak implosion velocity. The black lines show the interface between the ablator and the fuel. From left to right: Slow, Moderate, Fast, and Very Fast.

FIG. 20. Color-coded plot of density versus position from multimode simulations near ignition time. From left to right: Slow, Moderate, Fast, and Very Fast.

FIG. 21. The yield (MJ) versus ablator roughness (nm) assuming 1  $\mu\text{m}$  ice roughness from multimode simulations for the four capsules. Very Fast (dashed gray), Fast (solid black), Moderate (solid gray), and Slow (dashed black).

**TABLE 1. Parameters for the four indirectly driven capsules.**

Capsule	Very Fast	Fast	Moderate	Slow
Ablator radius (cm)	0.230	0.228	0.230	0.234
Outer fuel radius (cm)	0.205	0.203	0.205	0.209
Inner fuel radius (cm)	0.182	0.174	0.170	0.168
Mass of fuel (mg)	2.7	3.2	3.9	4.6
$v_{\text{imp-mw}}$ (107 cm/s)	3.1	2.8	2.5	2.3
Yield (MJ)	286	333	412	496
IFAR	50	45	38	26
Fuel energy/ $E_{\text{ign}}$	1.8	1.6	1.3	1.1

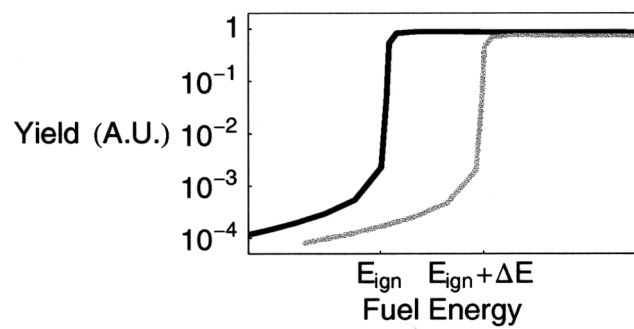


Figure 1

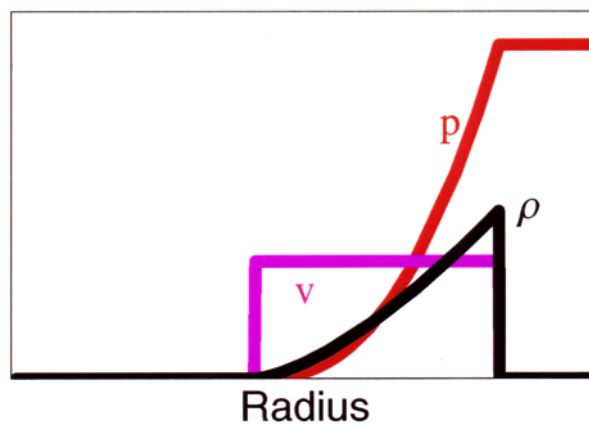
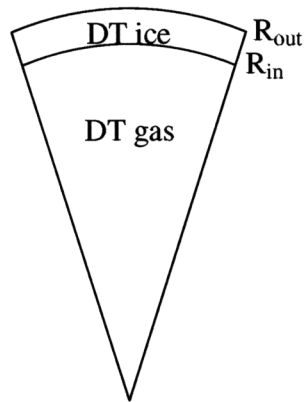
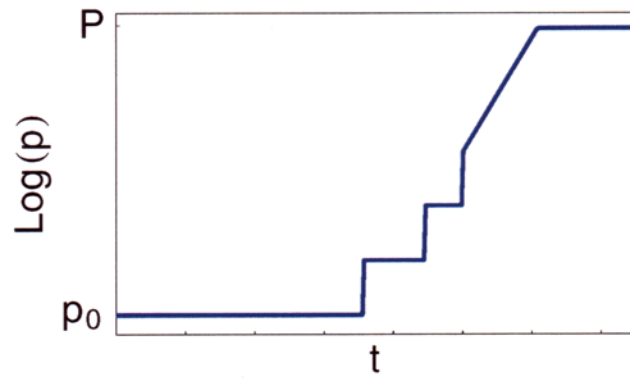


Figure 2



**Figure 3**



**Figure 4**

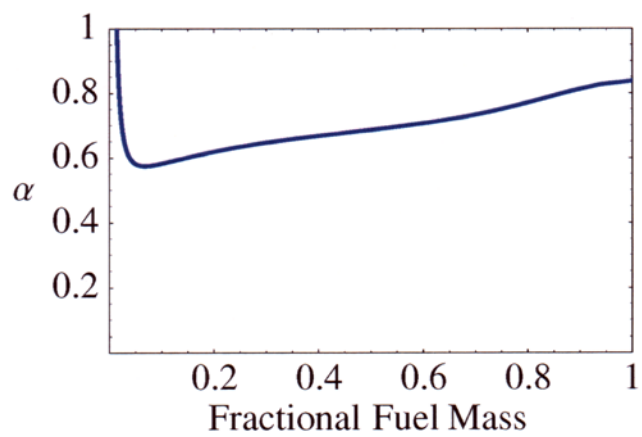


**Figure 5**

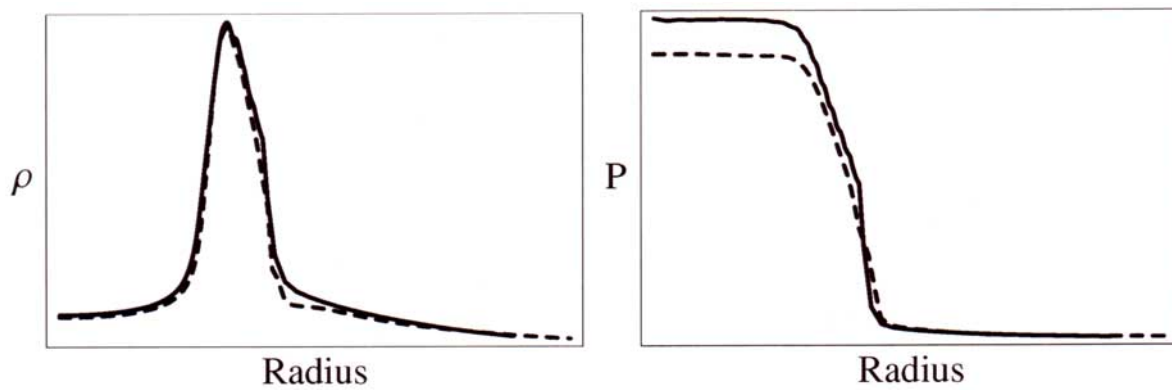


**Figure 6**

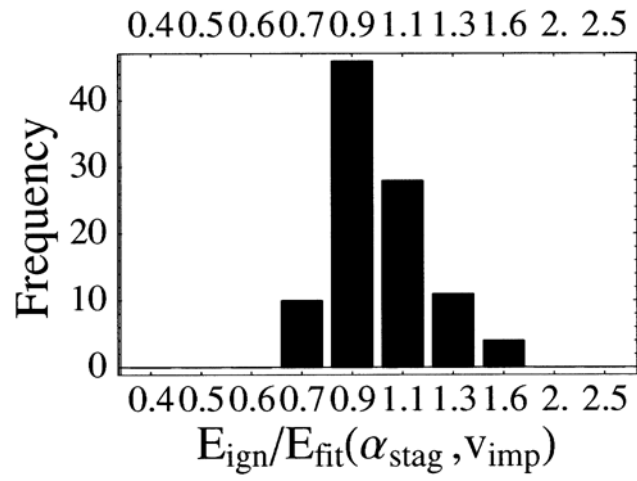


**Figure 7**

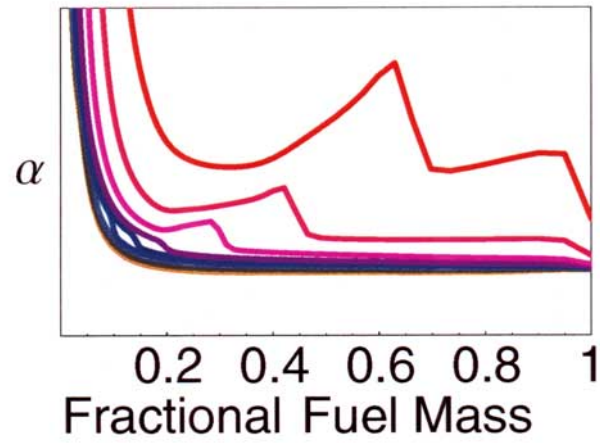


**Figure 8**

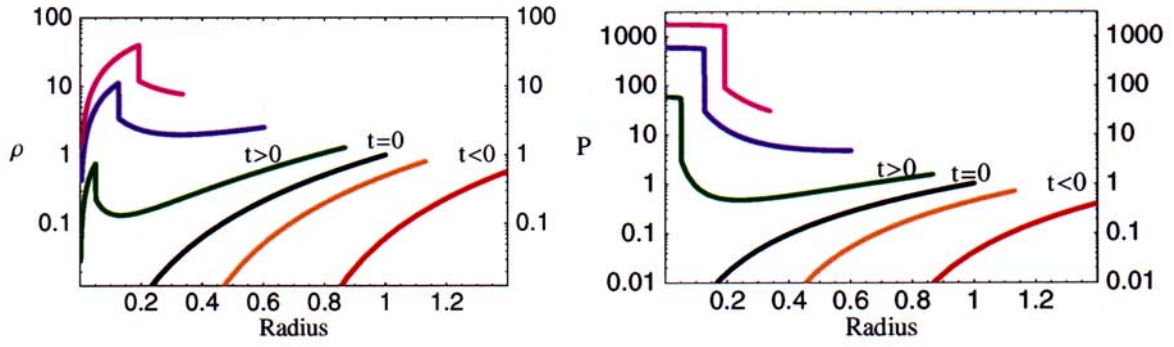


**Figure 9**

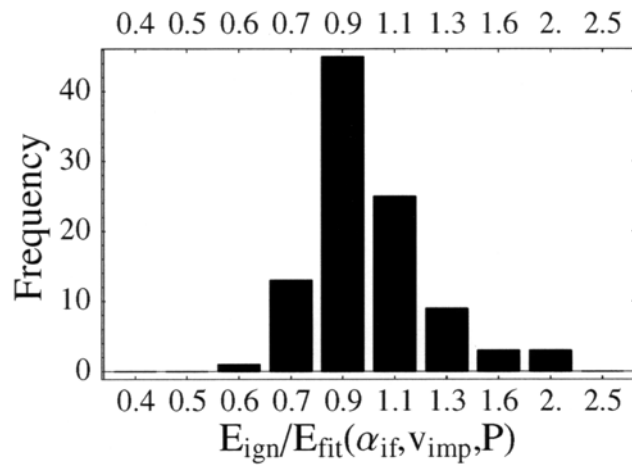


**Figure 10**

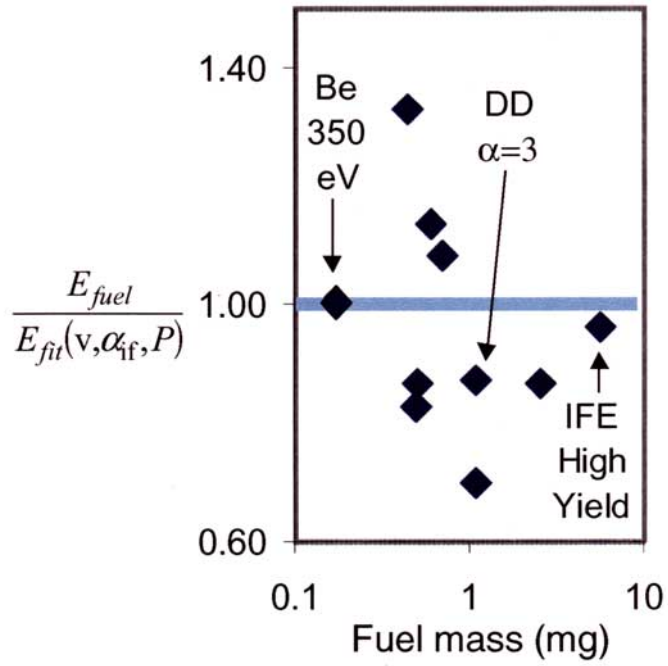


Figure 11`

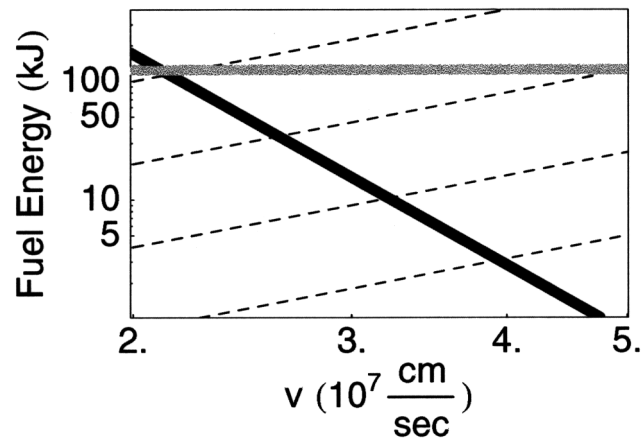
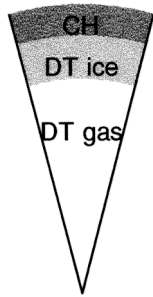
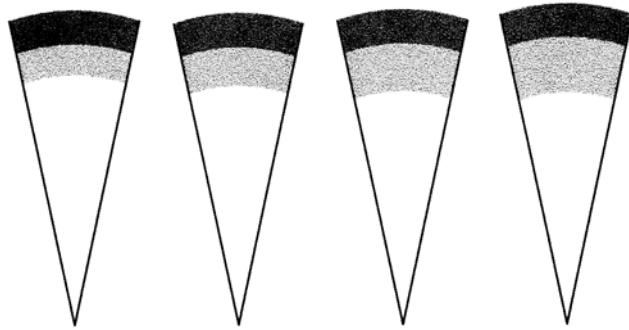


Figure 12`



**Figure 13**



**Figure 14**

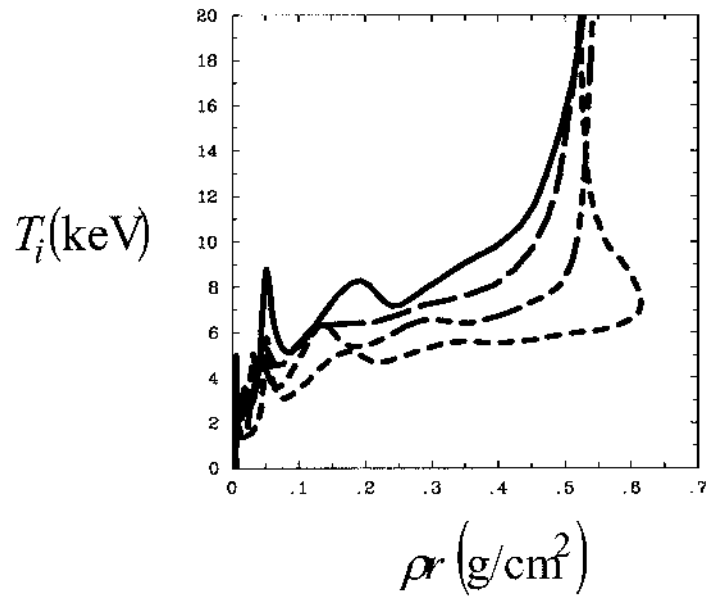


**Figure 15**

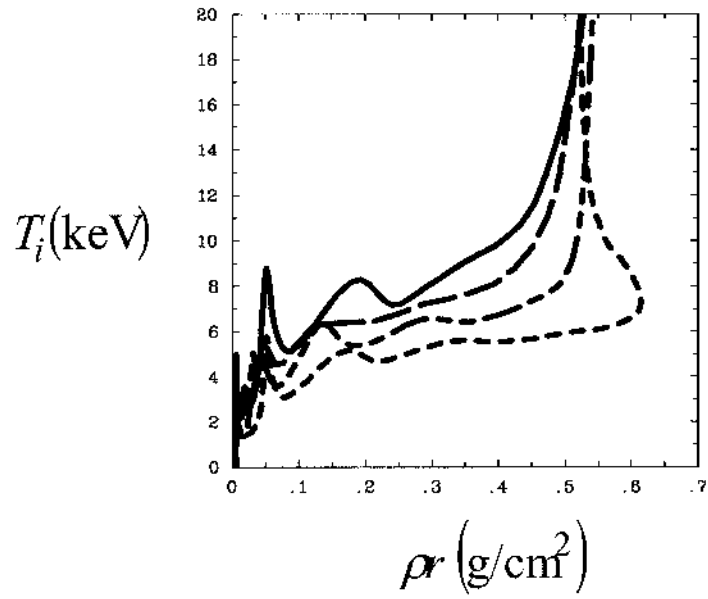


**Figure 16**

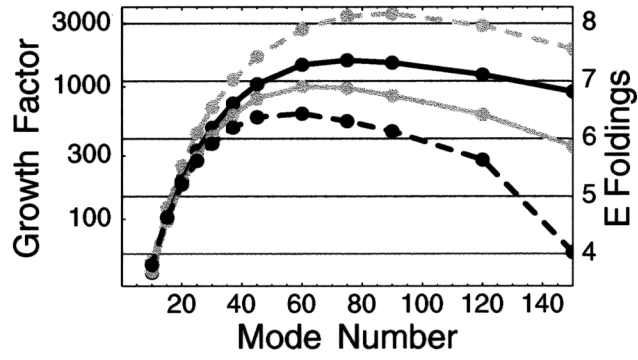


Figure 17

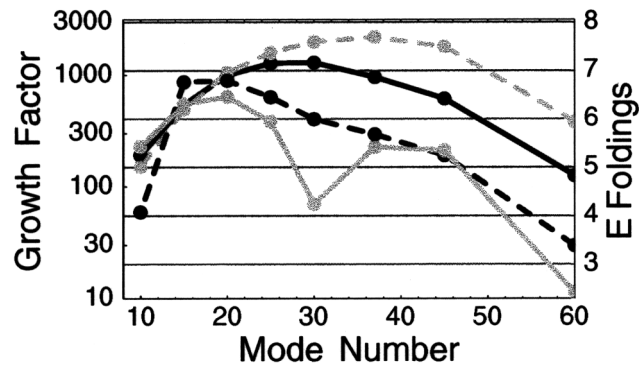
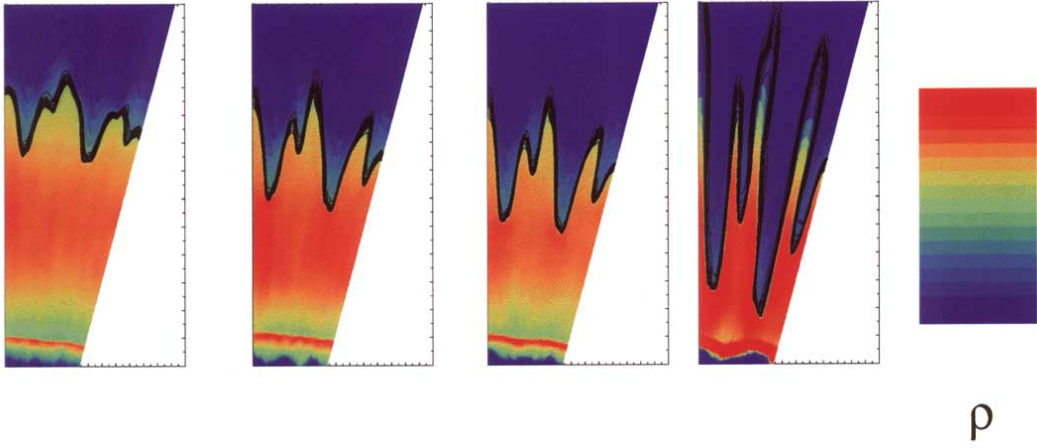
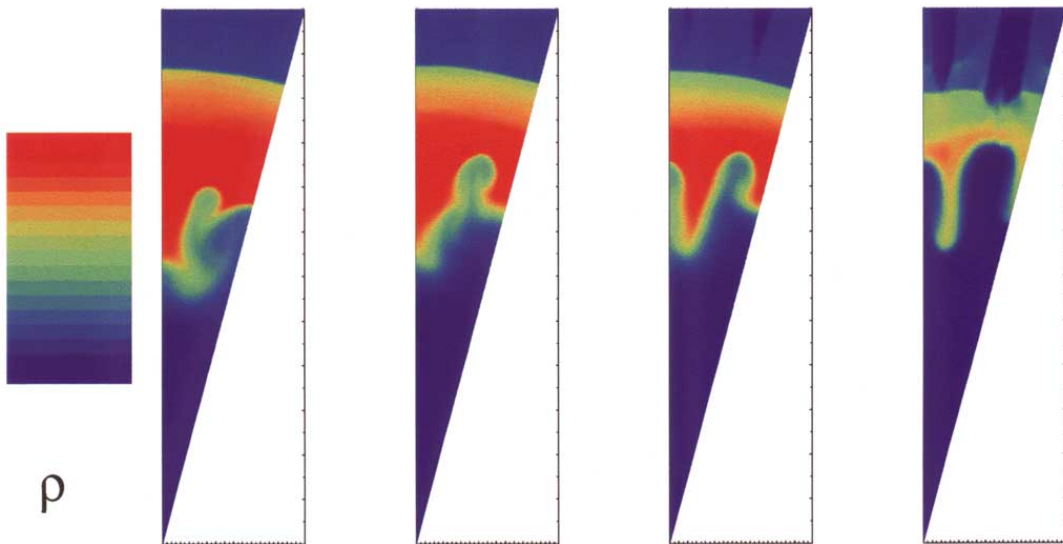


Figure 18



**Figure 19**



**Figure 20**

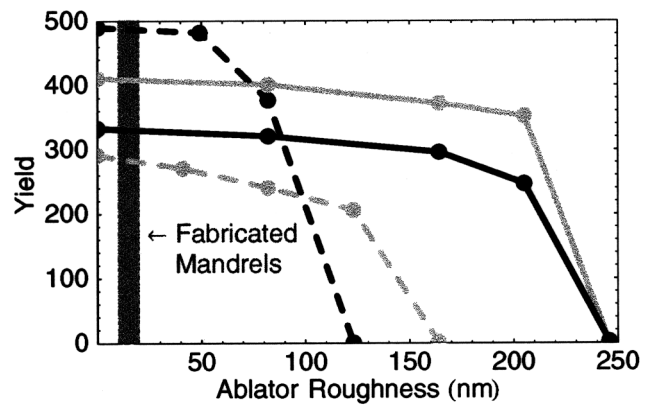


**Figure 21**